

Look Less, Reason More: Rollout-Guided Adaptive Pixel-Space Reasoning

Anonymous ACL submission

Abstract

Vision-Language Models (VLMs) excel at many multimodal tasks, yet they frequently struggle with tasks requiring precise understanding and handling of fine-grained visual elements. This is mainly due to information loss during image encoding or insufficient attention to critical regions. Recent work has shown promise by incorporating pixel-level visual information into the reasoning process, enabling VLMs to access high-resolution visual details during their thought process. However, this pixel-level information is often overused, leading to inefficiency and distraction from irrelevant visual details. To address these challenges, we propose the first framework for adaptive pixel reasoning that dynamically determines necessary pixel-level operations based on the input query. Specifically, we first apply operation-aware supervised fine-tuning to establish baseline competence in textual reasoning and visual operations, then design a novel rollout-guided reinforcement learning framework relying on feedback of the model’s own responses, which enables the VLM to determine when pixel operations should be invoked based on query difficulty. Experiments on extensive multimodal reasoning benchmarks show that our model achieves superior performance while significantly reducing unnecessary visual operations. Impressively, our model achieves 73.4% accuracy on HR-Bench 4K while maintaining a tool usage ratio of only 20.1%, improving accuracy and simultaneously reducing tool usage by 66.5% compared to the previous methods.

1 Introduction

Vision-Language Models (VLMs) have achieved remarkable progress, leveraging large language models and powerful vision encoders. Modern VLMs, such as GPT-4 (Hurst et al., 2024), Qwen-VL (Bai et al., 2025; Wang et al., 2024a), InternVL (Zhu et al., 2025; Wang et al., 2025b) and LLaVA (Li et al., 2024; Liu et al., 2023, 2024), can per-

form sophisticated visual understanding and reasoning tasks (Shen et al., 2025). However, VLMs frequently encounter difficulties in capturing fine-grained visual elements, largely because of information loss in the image encoding process or the limited allocation of attention to critical regions (Ge et al., 2024; He et al., 2024). Recently, advanced models (Su et al., 2025; Zhang et al., 2025b; Zheng et al., 2025; Zhou et al., 2025) have been proposed, which are capable of executing pixel-level operations—an ability we refer to as **pixel-space reasoning**. By zooming into specific regions, models can selectively focus on critical areas when the original image is too complex.

Existing models or frameworks that allow pixel-level operations can be broadly categorized into pipelining and end-to-end strategies. Pipelining approaches (Hu et al., 2024b; Lu et al., 2025; Liu et al., 2025; Li et al., 2025e) typically consist of multiple components, such as a predefined cropping tool or auxiliary feature extractors. While computationally efficient, they tend to leverage visual information more passively, rather than being actively shaped by the model’s reasoning needs. Therefore, they often fail to capture subtle but essential visual cues, especially in tasks requiring spatial reasoning or fine-grained perception. End-to-end strategies, in contrast, enable the model to actively manipulate visual inputs through pixel-level operations (Zheng et al., 2025; Zhou et al., 2025), such as zooming into specific regions.

Despite the flexibility of existing end-to-end methods (Wang et al., 2025a; Zhang et al., 2025a; Huang et al., 2025b), they often encourage the application of pixel-level operations regardless of whether the operations are actually needed. This overuse of pixel-level operations causes the following weaknesses: 1) **Computational inefficiency**: the frequent encoding of parts of the images requires additional time and slows down the inference speed. 2) **Learning difficulties**: cropped im-

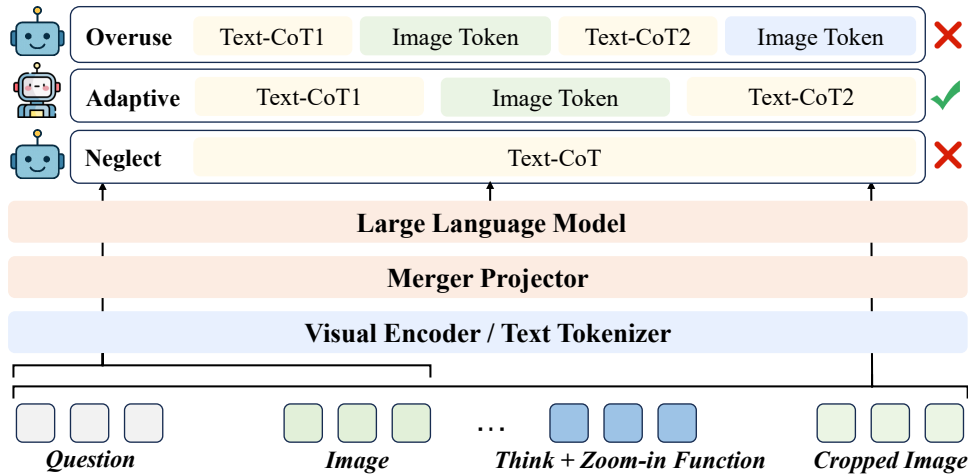


Figure 1: Comparison of different reasoning strategies. The “Overuse” strategy unnecessarily incorporates pixel-level operations, leading to inefficiency and potential distraction. The “Neglect” strategy relies solely on pure textual CoT reasoning, failing to engage with critical fine-grained visual details. Our “Adaptive” strategy achieves a balance by intelligently deciding whether to perform pixel-level operations based on the specific query, optimizing both accuracy and efficiency.

ages occupy substantial context space, potentially introducing noise and causing error propagation in the sequential generation process, particularly when cropped regions are irrelevant to the query. Ideally, a model should adaptively decide when to invoke pixel-level operations to focus more on relevant regions, and when a pure textual chain of thought (CoT) (Wei et al., 2022) alone suffices, thereby striking a balance between accuracy and efficiency. One straightforward solution is to have human experts manually label whether each query requires pixel-level operations, thereby providing additional supervision to guide the VLMs. However, this approach is both tedious and costly, making it impractical at scale. This naturally raises the question: can VLMs learn to apply pixel-level operations only when necessary, without relying on additional, predefined labels?

To address this, we propose the first framework for adaptive pixel-space reasoning that equips VLMs with the ability to dynamically determine the necessity of pixel-level operations. Since current open-source VLMs are rarely trained with pixel-level operations, we begin with **operation-aware supervised fine-tuning (SFT)** (§4.1), which provides the model with baseline competence in answering visual-related questions with or without pixel-level operations following specifications in the query. Afterwards, we design a novel **rollout-guided reinforcement learning (RGRL)** framework (§4.2) to enhance adaptive pixel-space reasoning capability. Unlike the conventional RL approach, which typically only promotes accuracy and encourages the frequency of tool usage, we

carefully design the reward assignment strategy to encourage the VLMs to leverage pixel reasoning only when it is beneficial. Our rollout-guided RL framework consists of two complementary components: (1) Pixel Necessity Rollouts, VLMs are explicitly required to produce answers both with and without pixel operations. The relative success rates provide implicit pixel operation necessity indicating whether pixel-level operations are beneficial for the query. (2) Adaptive Rollouts, which encourage VLMs to autonomously decide whether and how to apply pixel operations. Rewards are determined not only by the correctness of the responses, but also by their consistency with the necessity estimated in the previous rollouts. In this way, we promote efficient and robust adaptive pixel-space reasoning leveraging only the VLM’s own responses.

Extensive experiments show that our framework outperforms both general-purpose VLMs and strong tool-augmented baselines, achieving the highest average accuracy while minimizing unnecessary visual operations (§5.2). Specifically, our framework achieves 73.4% accuracy on HR-Bench 4K (Wang et al., 2024b) while maintaining a tool usage ratio of only 20.1%, improving accuracy and simultaneously reducing tool usage by 66.5% compared to the previous methods. Qualitative analysis further validates that our model can adaptively identify relevant visual regions and perform pixel operations only when contextually appropriate (??).

In summary, this work makes three key contributions: **1)** we introduce the first framework that enables adaptive pixel-space reasoning, allowing VLMs to determine when pixel-level operations

are necessary rather than applying them indiscriminately; 2) our training framework does not rely on any external pixel-level supervision or hand-crafted rules, allowing the model to estimate the necessity of pixel-level operations directly from its own reasoning process; 3) we achieve superior performance compared to baselines across five multimodal reasoning benchmarks while simultaneously improving reasoning accuracy and tool efficiency.

2 Related Work

Vision-Language Models. Vision-Language Models (VLMs) have evolved from early pipelines connecting visual encoders to frozen language models into more unified architectures trained with joint objectives. Representative frameworks such as BLIP-2 (Li et al., 2023) and LLaVA (Liu et al., 2023) employ connector modules—either projection layers (Li et al., 2025a; Cha et al., 2024) or attention-based adapters (Hu et al., 2023; Song et al., 2024)—to align image features with text embeddings, enabling tasks such as visual question answering and instruction following (Li et al., 2025c,d). Later research addresses perception bottlenecks, enhancing encoder capacity (Shen et al., 2024) or introducing dynamic resolution strategies (Anghelone et al., 2023). Open-source series (Wang et al., 2024a; Bai et al., 2025) and large-scale systems like Flamingo (Alayrac et al., 2022) and mPLUG-Owl (Ye et al., 2023, 2024) demonstrate competitive performance across multimodal benchmarks. Despite these developments, most models remain perception-centric, leaving room for improvements in complex reasoning.

Textual-space VLM Reasoning. Textual-space reasoning refers to approaches where VLMs improve reasoning by producing pure textual CoT, without directly manipulating pixels. Early works (Chen et al., 2023; Zhang et al., 2023) showed that inserting CoT steps enhances visual question answering. Follow-up methods refined this paradigm by improving rationale quality through self-consistency (Tan et al., 2023), dynamic routing (Aytes et al., 2025; Hu et al., 2025), or multi-image (Zhang et al., 2024; Xie et al., 2025) and relation-aware reasoning. Other directions emphasized interpretability via staged reasoning (Zheng et al., 2023) or automatic rationale generation to reduce annotation cost (Ma et al., 2024; Luo et al., 2024). Despite these advances, textual-space reasoning relies on static image embeddings and lacks

mechanisms to adaptively refine visual evidence, which motivates pixel-space reasoning approaches.

Pixel-space VLM Reasoning. Pixel-space reasoning, or “thinking with images,” refers to approaches where models actively manipulate visual inputs—such as cropping, masking, or sketching—rather than relying solely on pure textual CoT. Early attempts (Liu et al., 2025; Huang et al., 2025a; Lu et al., 2025) followed predefined workflows or required auxiliary annotations like spatial layouts, attributes, or external knowledge, which limited their generality. More recent tool-augmented frameworks (Su et al., 2025; Wang et al., 2025c; Zhang et al., 2025b; Zheng et al., 2025; Zhou et al., 2025) take a step toward interactive multimodal reasoning by enabling direct pixel-level operations. However, they often lack principled strategies for deciding when and how to invoke these operations (Feng et al., 2025; Li et al., 2025b), leading to inefficiency or distraction. These limitations motivate adaptive mechanisms that dynamically balance accuracy and efficiency. Unlike prior work that either hard-codes tool usage or overlooks its cost, our method explicitly learns when pixel-level operations are beneficial, achieving adaptive visual reasoning.

3 Problem Formulation

Multimodal reasoning involves solving queries that require varying degrees of pixel-level operations. While some queries can be accurately addressed using the model’s pure textual CoT, others demand focused pixel-level exploration to extract fine-grained information. This motivates *adaptive pixel-space reasoning*, where the model dynamically determines whether to invoke a pixel-level operation.

Formally, let $\mathbf{x} = [V, L]$ denote a vision-language query, with V representing the visual input and L the textual instruction. The model generates a reasoning trajectory $\mathbf{y} = [y_1, \dots, y_n, \hat{a}]$, where each step y_t can be either a pure textual CoT or a zoom-in operation, and \hat{a} is the model’s final predicted answer. The zoom-in operation extracts high-resolution information from a specified region of V , which is then incorporated into the subsequent reasoning steps: $y_t \leftarrow \text{concat}(y_t, f_{\text{zoom-in}}(y_t))$, where $f_{\text{zoom-in}}(y_t)$ denotes the high-resolution visual features acquired by the zoom-in operation.

To evaluate solution correctness, we compare the predicted answer \hat{a} with the ground-truth answer

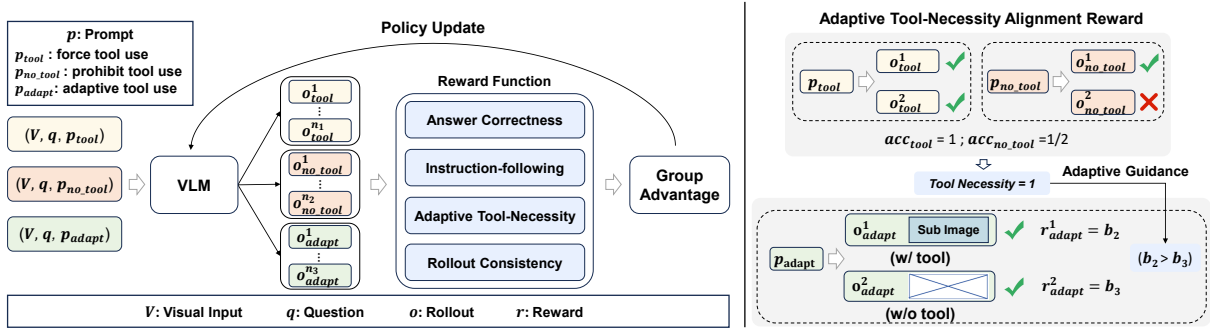


Figure 2: Overview of rollout-guided reinforcement learning. The framework generates rollouts under three prompting modes: forced tool use, prohibited tool use, and adaptive tool use, and these rollouts are rewarded by multiple reward functions. The adaptive tool-necessity alignment reward leverages comparisons between tool and no-tool rollouts to determine pixel tool necessity and guide the adaptive rollout, where the reward is determined by the model’s own adaptive reasoning and match of tool necessity. All rewards are aggregated to compute group advantage, which updates the policy to achieve efficient and adaptive visual reasoning.

α^* and define the reward:

$$r_{\text{correct}}(\mathbf{x}, \mathbf{y}) = \begin{cases} 1 & \text{if } \hat{a} = a^*, \\ 0 & \text{otherwise.} \end{cases} \quad (1)$$

The overall objective of RL training can then be written as

$$\max_{\theta} E_{\mathbf{x} \sim \mathcal{D}, \mathbf{y} \sim \pi_{\theta}(\mathbf{y}|\mathbf{x})} [R(\mathbf{x}, \mathbf{y})], \quad (2)$$

$$R(\mathbf{x}, \mathbf{y}) = r_{\text{correct}}(\mathbf{x}, \mathbf{y}) + \lambda r_{\text{pixel}}(\mathbf{x}, \mathbf{y}), \quad (3)$$

where $r_{\text{pixel}}(\mathbf{x}, \mathbf{y})$ provides a positive reward if a pixel-level operation improves the final answer \hat{a} and a negative reward if it is unnecessary or detrimental, and λ controls the trade-off between correctness and efficiency.

Under this formulation, the model must develop a query-specific adaptive strategy: it should invoke zoom-in selectively, only when pixel-level operations contribute to the final solution. By explicitly considering the benefit of visual operations, the framework encourages accurate, efficient, and robust reasoning across diverse query complexities.

4 Method

Existing RL methods for pixel-space reasoning often fail to learn an adaptive strategy, leading to two common failure modes: either an over-reliance on zoom-in or a complete avoidance of it. To address this, we propose an **adaptive rollout-guided RL training framework** that enables dynamic decision-making for visual exploration. Our method consists of two primary stages: operation-aware SFT phase (§4.1) and rollout-guided reinforcement learning (RGRL) phase (§4.2).

4.1 Operation-Aware Supervised Fine-Tuning

We begin with a supervised training stage on \mathcal{D}_{SFT} , a dataset that not only provides question-answer pairs but also their detailed reasoning trajectories. These trajectories are operation-aware: a portion of them involves explicit pixel-level operations, while others rely purely on textual CoT. By exposing the model to both categories, this stage enables it to establish foundational competence in both pure textual CoT and the proper execution of visual operations. It effectively prepares the model for the more complex adaptive RGRL stage by having it minimize a standard cross-entropy loss:

$$\mathcal{L}_{\text{SFT}} = - \sum_{(\mathbf{x}_i, \mathbf{y}_i) \in \mathcal{D}_{\text{SFT}}} \log P_{\theta}(\mathbf{y}_i | \mathbf{x}_i), \quad (4)$$

where \mathbf{x}_i denotes the input query, \mathbf{y}_i is the reasoning trajectory, and θ is the model parameters.

4.2 Rollout-guided Reinforcement Learning

After the SFT training, we transition to rollout-guided RL, where the model learns to achieve adaptive pixel-space reasoning. For each vision-language query $\mathbf{x} = [V, L]$, we perform a total of N reasoning rollouts. These rollouts are strategically divided into two groups: *pixel necessity rollouts*, which evaluate the necessity of zoom-in and provide an implicit tool necessity signal, and *adaptive rollouts*, where the model learns to make its own informed decisions. To control the model’s behavior during each rollout, we prepend a specific system prompt in the textual instruction L .

4.2.1 Pixel Necessity Rollouts

The first $N_{\text{necessity}} = n_1 + n_2$ rollouts are controlled to estimate the query-specific necessity of

invoking zoom-in. We achieve this by using different system prompts. For the first n_1 rollouts, we use system prompt p_{tool} to force a tool-use action. For the next n_2 rollouts, we use system prompt $p_{\text{no_tool}}$ to prohibit tool use. This setup provides two distinct performance baselines: one with pixel operation and one with only pure textual CoT. We then compare the average accuracy of these two groups, acc^{tool} and $acc^{\text{no_tool}}$, to determine a query-specific adaptive tool necessity. Let $\mathbf{1}_{\text{tool_necessity}}$ denotes the indicator of the necessity to use pixel-space operations (1 if necessary, 0 otherwise). This tool necessity provides a crucial guidance signal for subsequent learning:

$$\mathbf{1}_{\text{tool_necessity}} = \begin{cases} 1 & \text{if } acc^{\text{no_tool}} < acc^{\text{tool}}, \\ 0 & \text{otherwise.} \end{cases} \quad (5)$$

Instruction-following Reward. During the pixel necessity estimation phase, we apply an *instruction-following reward* to ensure the model follows the enforced system prompt for the entire reasoning trajectory. Let $\mathbf{z} = [z_1, \dots, z_m]$ denote the sequence of pixel-level actions in the trajectory, and let $\mathcal{Z}^{\text{prompt}} \subset \{0, 1\}$ be the set of allowed actions according to the current prompt ($\{1\}$ for forced zoom-in, $\{0\}$ for prohibited zoom-in). We define the reward as

$$r_{\text{instr}} = \begin{cases} +b_1, & \text{if } \exists t \text{ s.t. } z_t \in \mathcal{Z}^{\text{prompt}}, \\ -c_1, & \text{otherwise,} \end{cases} \quad (6)$$

where $b_1, c_1 > 0$ are positive constants. That is, the trajectory receives a positive reward if it contains at least one action allowed by the prompt, and a negative reward otherwise.

4.2.2 Adaptive Rollouts

The remaining $N_{\text{adaptive}} = n_3$ rollouts allow the model to learn adaptive strategy. For these attempts, a neutral system prompt p_{adapt} is used, letting the model freely decide whether to invoke a zoom-in operation. Each adaptive rollout guides the model to learn an efficient, query-specific strategy. For detailed prompts, please refer to Appendix A.

Adaptive Tool-Necessity Alignment Reward. This reward encourages the model to align its zoom-in decisions with the query-specific tool necessity obtained from the pixel necessity rollouts. Let $\mathbf{1}_{\text{zoom}} \in \{0, 1\}$ denote whether a zoom-in operation is performed during the thought process (1 if performed, else 0), $\mathbf{1}_{\text{correct}} \in \{0, 1\}$

indicate whether the final answer is correct, and $m = \mathbf{1}[\mathbf{1}_{\text{zoom}} = 1 \iff \mathbf{1}_{\text{tool_necessity}} = 1]$ represent whether the zoom decision matches the query-specific necessity ($m = 1$ if matched, else $m = 0$). We define the adaptive tool-necessity alignment reward as:

$$r = \begin{cases} +b_2, & \text{if } \mathbf{1}_{\text{correct}} = 1 \text{ and } m = 1, \\ +b_3, & \text{if } \mathbf{1}_{\text{correct}} = 1 \text{ and } m = 0, \\ -c_2, & \text{if } \mathbf{1}_{\text{correct}} = 0 \text{ and } m = 1, \\ -c_3, & \text{if } \mathbf{1}_{\text{correct}} = 0 \text{ and } m = 0, \end{cases} \quad (7)$$

where $b_2, c_2, b_3, c_3 > 0$ are positive real numbers, with $b_2 > b_3$ and $c_3 > c_2$. Intuitively, the reward separates two factors: (i) whether the zoom decision matches the query-specific necessity, and (ii) whether the final answer is correct. If the model follows the query-specific necessity *and* produces a correct answer, it receives $+b_2$; if it follows the guidance but the answer is incorrect, it receives $-c_2$; if it does not follow the guidance but still answers correctly, it receives $+b_3$; otherwise it receives $-c_3$. We evaluate two dimensions—adherence and correctness. Since the reward for being both adherent and correct should exceed that for being correct despite non-adherence, we set $b_2 > b_3 > 0$. Moreover, the case associated with c_3 corresponds to simultaneous non-adherence and incorrectness; hence it incurs the largest penalty, with $c_3 > c_2 > 0$. Together, these constraints encourage both correctness and adherence to the tool-necessity guidance.

Rollout Consistency Reward. To encourage stable decisions across rollouts of the same query, we penalize inconsistent tool usage among the N_{adaptive} adaptive rollouts:

$$r_{\text{cons}} = -\gamma \text{Var}(\mathbf{1}_{\text{zoom}}), \quad \gamma > 0. \quad (8)$$

The $\text{Var}(\mathbf{1}_{\text{zoom}})$ measures the variability of tool usage, with lower variance corresponding to more consistent decisions.

4.2.3 Overall Rollout-Guided Reward

The overall objective is to maximize a unified reward R , which is realized differently in the two rollout phases: $R_{\text{necessity}}$ for pixel necessity rollouts and R_{adapt} for adaptive rollouts.

For the *pixel necessity rollouts*, the reward combines correctness and instruction-following:

$$R_{\text{necessity}} = r_{\text{correct}} + \lambda_{\text{instr}} r_{\text{instr}}, \quad (9)$$

Table 1: Performance and tool usage ratio of models on five multimodal reasoning benchmarks. Numbers in the top row indicate Accuracy (or ANLS for InfoVQA), while the **gray numbers in parentheses** indicate the corresponding **tool usage ratio (%)**. * denotes results reproduced by ourselves, † denotes methods using GPT-4V.

Model	Size	V* Bench	MMStar	HR-Bench 4K	HR-Bench 8K	InfoVQA	Avg
Model w/o Tools							
GPT-4o	-	62.8	61.6	59.0	55.5	80.7	63.9
Gemini-2.0-Flash	-	73.2	-	-	-	86.5	-
Gemini-2.5-Pro	-	79.2	-	-	-	84.0	-
LLaVA-OneVision	7B	75.4	61.7	63.0	59.8	68.8	65.7
DeepSeek-VL	7B	-	40.5	35.5	33.4	-	-
IXC2-4KHD	7B	-	-	57.8	51.3	68.6	-
Video-R1	7B	51.2	-	-	-	67.9	-
LongLLava	13B	68.5	-	-	-	65.4	-
Gemma3	27B	62.3	-	-	-	59.4	-
Qwen2.5-VL*	7B	73.3	63.6	67.3	64.1	78.5	69.4
Model w/ Tools							
IVM-Enhance†	-	81.2	-	-	-	-	-
SEAL	7B	74.8	-	-	-	-	-
PaLI-X-VPD	55B	76.6	-	-	-	-	-
Pixel Reasoner*	7B	84.3 (80.7)	63.4 (47.1)	72.6 (86.6)	66.1 (87.4)	83.9 (25.1)	74.1 (65.4)
Ours	7B	85.9 (59.1) _{-21.6}	64.3 (37.9) _{-9.2}	73.4 (20.1) _{-66.5}	66.6 (48.5) _{-38.9}	84.4 (14.6) _{-10.5}	74.9 (36.0) _{-29.4}

where $\lambda_{\text{instr}} > 0$ controls the relative importance of following the prompt versus answering correctly.

For the *adaptive rollouts*, the reward incorporates three components, guiding the model towards an optimal, stable, and adaptive strategy:

$$R_{\text{adapt}} = r_{\text{correct}} + \lambda_{\text{align}} r_{\text{align}} + r_{\text{cons}}, \quad (10)$$

where $\lambda_{\text{align}} > 0$ balances the influence of the adaptive tool-necessity alignment reward relative to correctness and consistency.

5 Experiments

5.1 Setups

Training.

We follow Pixel-Reasoner (Su et al., 2025) and use its datasets, comprising 4k samples for SFT and 7k samples for RL. The base model is Qwen2.5-VL-7B-Instruct (Bai et al., 2025). We adopt Open-R1 (Hugging Face, 2025) for SFT and OpenRLHF (Hu et al., 2024a) for RL. For SFT, we use a batch size of 128 and a learning rate of 1×10^{-6} . For RL, we employ a cosine learning rate schedule with a learning rate of 1×10^{-6} . Each batch samples 256 prompts, with $N = 16$ rollouts per prompt ($n_1 = 4$, $n_2 = 4$ and $n_3 = 8$), allowing at most 3 pixel-level operations. We provide detailed hyperparameters in the Appendix B.

Baseline. We compare our approach with general-purpose and tool-augmented VLMs. The first group includes representative VLMs such as GPT-4o (Hurst et al., 2024), Gemini-2.5 series (Team et al., 2024; Comanici et al., 2025;

Team et al., 2023), LLaVA-OneVision (Li et al., 2024), DeepSeek-VL (Lu et al., 2024), InternLM-XComposer2-4KHD (IXC2-4KHD) (Dong et al., 2024), Qwen2.5-VL (Bai et al., 2025), Video-R1 (Feng et al., 2025), LongLLaVA (Wang et al., 2024c), and Gemma3 (Team et al., 2025). These models directly perform reasoning without external tool invocation. The second group consists of tool-augmented models, including Instruction-Guided Masking (IVM-Enhance) (Zheng et al., 2024), Visual-Program-Distillation (PaLI-X-VPD) (Hu et al., 2024b), SEAL (Wu and Xie, 2024), and Pixel Reasoner (Su et al., 2025), which represents a strong baseline for pixel-space reasoning with its innovative approach to zoom-in visual operations.

Benchmark. We evaluate our method across five diverse multimodal benchmarks, covering general, fine-grained perception and complex high-level reasoning including V* Bench (Wu and Xie, 2024), MMStar (Chen et al., 2024), HR-Bench (4K/8K) (Wang et al., 2024b) and InfographicVQA (InfoVQA) (Mathew et al., 2022). Among these benchmarks, all adopt Accuracy metrics for evaluation except InfoVQA, which uses the Average Normalized Levenshtein Similarity (ANLS).

5.2 Main Results

Our method achieves consistent superior performance on multimodal reasoning benchmarks, outperforming both general VLMs and strong tool-augmented VLMs. As shown in Table 1, compared to existing baselines, our method

Table 2: Ablation study on the effectiveness of rollout-guided RL.

Model	V* Bench	MMStar	HR-Bench 4K	HR-Bench 8K	InfoVQA	Avg
Ours w/o RGRL	78.5 (9.4)	58.4 (39.3)	66.6 (68.8)	57.0 (65.3)	73.9 (20.1)	66.9 (40.6)
Ours	85.9 (59.1)	64.3 (37.9)	73.4 (20.1)	66.6 (48.5)	84.4 (14.6)	74.9 (36.0)

Table 3: Ablation study of different tool usage strategies.

Model	V* Bench	MMStar	HR-Bench 4K	HR-Bench 8K	InfoVQA	Avg
All No-Tool	81.2	63.8	70.9	63.8	82.1	72.4
All Tool	83.2	63.5	71.3	62.6	81.7	72.5
Ours	85.9	64.3	73.4	66.6	84.4	74.9

achieves the highest average score. Both our method and Pixel Reasoner are trained based on Qwen2.5-VL under comparable data settings. While Pixel Reasoner exhibits performance degradation on MMStar due to indiscriminate pixel-level operations, our method maintains consistent superior performance across all five benchmarks. This demonstrates that our adaptive framework can effectively determine when pixel-level operations are truly necessary, avoiding redundant computations while preserving accuracy.

Adaptive tool usage significantly reduces unnecessary visual operations without sacrificing accuracy. We further analyze the tool usage ratio across benchmarks in Table 1. The result shows that our model adaptively balances pure textual CoT and pixel-level operations assistance, achieving an average tool ratio of 36.0%, substantially lower than the existing strong tool-augmented baseline Pixel Reasoner (65.4%). The lower overall average ratio primarily reflects our ability to avoid redundant tool invocations, indicating that the model not only achieves better accuracy but also reduces unnecessary computational overhead.

Adaptive reasoning capabilities emerge through Rollout-Guided RL training. The task-dependent distribution of the tool usage ratio provides strong evidence that our framework has successfully trained the model to possess adaptive reasoning capabilities. Our model naturally invokes fewer tools on relatively simple benchmarks (e.g., InfoVQA, tool ratio 14.6%) while increasing tool reliance on more challenging benchmarks (e.g., HR-Bench 8K, tool ratio 48.5%), demonstrating that the learned adaptive behavior aligns with the actual reasoning demands of queries. Besides, as shown in Table 2, our RGRL training can effectively correct redundant tool usage patterns learned during SFT. For instance, on InfoVQA, the model initially exhibits excessive tool usage (20.1%) after SFT, but our RL

training successfully reduces this to 14.6%, while simultaneously improving accuracy from 73.9% to 84.4%. We provide some representative cases in the Appendix D.

5.3 Ablation Study

5.3.1 Effectiveness of Rollout-Guided RL

We also evaluate our model without the RGRL phase, relying solely on operation-aware SFT. As shown in Table 2, without RL training, the variant exhibits a significantly lower accuracy and higher tool usage compared to our full approach. These results suggest that, while SFT alone provides foundational capability, it lacks the ability to dynamically adjust tool usage based on the complexity of the task. This reinforces the effectiveness of combining operation-aware SFT with RGRL to enhance the model’s adaptive decision-making in multimodal reasoning tasks.

5.3.2 Comparison of Tool Usage Strategies

The results of the ablation study, which evaluates our trained model under different tool usage prompts, are shown in Table 3. The first two rows correspond to extreme cases: **All No-Tool**, where the model relies solely on pure textual CoT, and **All Tool**, where the model always uses pixel-level operations. The All No-Tool strategy achieves an average accuracy of 72.4 across the five benchmarks, while the All Tool strategy achieves 72.5. Both are lower than our adaptive method, which reaches an average accuracy of 74.9. The All-Tool strategy underperforms particularly on high-resolution benchmarks such as HR-Bench 8K, showing that excessive reliance on pixel-level operations can be counterproductive. Frequent zoom-in operations lead to redundant cropping, which introduces noisy visual paths and distracts the reasoning process. Similarly, the All No-Tool strategy cannot fully exploit the benefits of visual operations in complex scenarios, as it can’t zoom into critical regions and

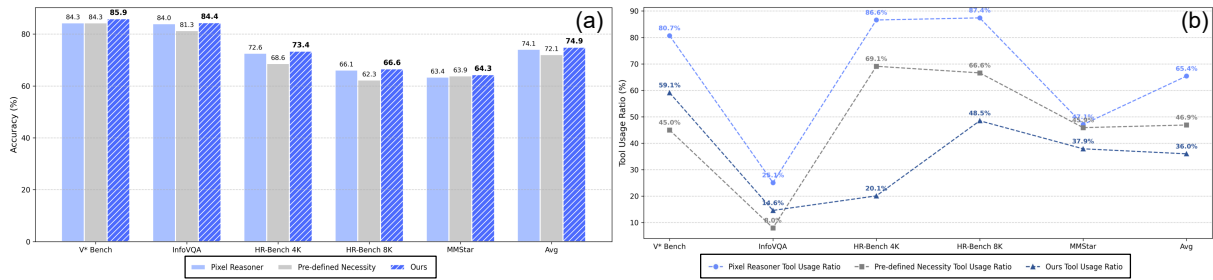


Figure 3: Ablation study on the effectiveness of pixel necessity estimation, showing benchmark accuracy (a) and tool usage ratio (b).

Table 4: Ablation study on the effectiveness of rewards in the pixel necessity rollouts.

Model	V* Bench	MMStar	HR-Bench 4K	HR-Bench 8K	InfoVQA	Avg
Ours w/o PN rewards	85.3 (68.1)	64.0 (54.9)	73.1 (21.9)	64.0 (39.0)	82.1 (1.9)	73.7 (37.2)
Ours	85.9 (59.1)	64.3 (37.9)	73.4 (20.1)	66.6 (48.5)	84.4 (14.6)	74.9 (36.0)

extract fine-grained visual cues. In contrast, our adaptive method determines dynamically when tool usage is beneficial, leading to the highest accuracy on all five benchmarks.

5.3.3 Effectiveness of Necessity Estimation

We further evaluate the effect of dynamically determining tool usage necessity in pixel necessity rollouts compared to using predefined necessity. The predefined necessity is obtained by running our SFT model with a temperature of 1.0 and collecting 8 rollouts per query (Pass@8); for each query, if the majority of rollouts involve tool usage, the necessity is set to “tool,” otherwise to “no-tool”. Figure 3 (a) shows the accuracy across five benchmarks. The predefined necessity approach achieves an average accuracy of 72.1, which is lower than Pixel Reasoner (Su et al., 2025) and significantly below our adaptive method. This demonstrates that static necessity assignment cannot adapt to changes in the model’s capability and thus fails to reliably estimate whether a query requires tool usage during the training process, leading to substantial accuracy loss. The performance gap is most pronounced on HR-Bench 4K/8K, where predefined necessity reduces the model’s ability to handle high-resolution visual reasoning. Figure 3 (b) reports the ratio of tool usage across benchmarks. Although predefined necessity produces a tool ratio of 46.9, falling between Pixel Reasoner and our method, it fails to deliver the same accuracy improvements. This indicates that while predefined necessity reduces redundant visual operations compared to Pixel Reasoner, they cannot match the flexibility of adaptive reasoning. Our adaptive strategy enables the model

to make decisions about when to invoke tools, improving both accuracy and efficient tool utilization.

5.3.4 Effectiveness of Rewards in Necessity Rollouts

Table 4 evaluates the effectiveness of incorporating rewards from the pixel necessity rollouts during RGRL. When the rewards from the first eight rollouts (forced tool and forced no-tool) are excluded from gradient updates (Ours w/o PN rewards), the model attains an average accuracy of 73.7 across the five benchmarks. Incorporating these rewards consistently improves performance, with our full method reaching 74.9 on average. These results confirm that the rewards in pixel necessity rollouts provide reliable tool necessity for learning when tool usage is truly beneficial, which subsequently enhances the adaptive rollouts.

6 Conclusion

In this work, we introduced a framework for adaptive pixel-space reasoning in multimodal reasoning tasks. By combining operation-aware supervised fine-tuning with rollout-guided reinforcement learning, the model learns query-specific strategies for deciding when to invoke pixel-level operations. Compared to other pipelining and end-to-end multimodal reasoning methods, the proposed approach demonstrates the ability to dynamically adapt to varying query complexities, avoiding both neglect and overuse of pixel-level operations. Extensive experiments across five benchmarks confirm that this framework consistently improves accuracy and efficiency, validating the effectiveness of our adaptive pixel-space reasoning framework.

610 Limitations

611 The limitations of this work primarily stem from
612 the restricted scope of pixel operations. Although
613 our proposed rollout-guided reinforcement learning
614 framework is tool-agnostic in its design, abstract-
615 ing the decision as a “tool vs. no-tool” choice,
616 and its reward mechanism does not rely on the
617 specific semantics of any single operation, our em-
618 pirical validation is exclusively focused on a single
619 pixel-space operation: zoom-in. This choice was
620 motivated by the need for fair and standardized
621 comparison with prior literature. Future work will
622 concentrate on extending our framework to incor-
623 porate a wider array of pixel-space operations and
624 exploring robust multi-tool coordination within our
625 adaptive reasoning design.

626 References

627 Jean-Baptiste Alayrac, Jeff Donahue, Pauline Luc,
628 Antoine Miech, Iain Barr, Yana Hasson, Karel
629 Lenc, Arthur Mensch, Katherine Millican, Malcolm
630 Reynolds, and 1 others. 2022. Flamingo: a visual
631 language model for few-shot learning. *Advances in*
632 *neural information processing systems*, 35:23716–
633 23736.

634 David Anghelone, Sarah Lannes, and Antitza Dantcheva.
635 2023. Anyres: Generating high-resolution visible-
636 face images from low-resolution thermal-face images.
637 In *2023 IEEE International Conference on Multime-*
638 *dia and Expo (ICME)*, pages 246–251. IEEE.

639 Simon A Aytes, Jinheon Baek, and Sung Ju Hwang.
640 2025. Sketch-of-thought: Efficient llm reasoning
641 with adaptive cognitive-inspired sketching. *arXiv*
642 *preprint arXiv:2503.05179*.

643 Shuai Bai, Keqin Chen, Xuejing Liu, Jialin Wang, Wen-
644 bin Ge, Sibao Song, Kai Dang, Peng Wang, Shijie
645 Wang, Jun Tang, and 1 others. 2025. Qwen2. 5-vl
646 technical report. *arXiv preprint arXiv:2502.13923*.

647 Junbum Cha, Wooyoung Kang, Jonghwan Mun, and
648 Byungseok Roh. 2024. Honeybee: Locality-
649 enhanced projector for multimodal llm. In *Proceed-*
650 *ings of the IEEE/CVF Conference on Computer Vi-*
651 *sion and Pattern Recognition*, pages 13817–13827.

652 Lin Chen, Jinsong Li, Xiaoyi Dong, Pan Zhang, Yuhang
653 Zang, Zehui Chen, Haodong Duan, Jiaqi Wang,
654 Yu Qiao, Dahua Lin, and 1 others. 2024. Are we
655 on the right way for evaluating large vision-language
656 models? *Advances in Neural Information Processing*
657 *Systems*, 37:27056–27087.

658 Zhenfang Chen, Qinlong Zhou, Yikang Shen, Yining
659 Hong, Hao Zhang, and Chuang Gan. 2023. See,
660 think, confirm: Interactive prompting between vision
661 and language models for knowledge-based visual
662 reasoning. *arXiv preprint arXiv:2301.05226*.

Gheorghe Comanici, Eric Bieber, Mike Schaeckermann,
Ice Pasupat, Noveen Sachdeva, Inderjit Dhillon, Mar-
cel Blistein, Ori Ram, Dan Zhang, Evan Rosen, and
1 others. 2025. Gemini 2.5: Pushing the frontier with
advanced reasoning, multimodality, long context, and
next generation agentic capabilities. *arXiv preprint*
arXiv:2507.06261. 663
664
665
666
667
668
669

Xiaoyi Dong, Pan Zhang, Yuhang Zang, Yuhang
Cao, Bin Wang, Linke Ouyang, Songyang Zhang,
Haodong Duan, Wenwei Zhang, Yining Li, and 1
others. 2024. Internlm-xcomposer2-4khd: A pioneer-
ing large vision-language model handling resolutions
from 336 pixels to 4k hd. *Advances in Neural Infor-*
mation Processing Systems, 37:42566–42592. 670
671
672
673
674
675
676

Kaituo Feng, Kaixiong Gong, Bohao Li, Zonghao Guo,
Yibing Wang, Tianshuo Peng, Junfei Wu, Xiaoy-
ing Zhang, Benyou Wang, and Xiangyu Yue. 2025.
Video-r1: Reinforcing video reasoning in mllms.
arXiv preprint arXiv:2503.21776. 677
678
679
680
681

Chunjiang Ge, Sijie Cheng, Ziming Wang, Jiale Yuan,
Yuan Gao, Jun Song, Shiji Song, Gao Huang, and
Bo Zheng. 2024. Convllava: Hierarchical backbones
as visual encoder for large multimodal models. *arXiv*
preprint arXiv:2405.15738. 682
683
684
685
686

Xin He, Longhui Wei, Lingxi Xie, and Qi Tian. 2024.
Incorporating visual experts to resolve the informa-
tion loss in multimodal large language models. *arXiv*
preprint arXiv:2401.03105. 687
688
689
690

Jian Hu, Xibin Wu, Wei Shen, Jason Klein Liu, Zilin
Zhu, Weixun Wang, Songlin Jiang, Haoran Wang,
Hao Chen, Bin Chen, and 1 others. 2024a. Openrlhf:
An easy-to-use, scalable and high-performance rlhf
framework. *arXiv preprint arXiv:2405.11143*. 691
692
693
694
695

Wanpeng Hu, Haodi Liu, Lin Chen, Feng Zhou,
Changming Xiao, Qi Yang, and Changshui Zhang.
2025. Socratic questioning: Learn to self-guide
multimodal reasoning in the wild. *arXiv preprint*
arXiv:2501.02964. 696
697
698
699
700

Yushi Hu, Otilia Stretcu, Chun-Ta Lu, Krishnamurthy
Viswanathan, Kenji Hata, Enming Luo, Ranjay Kr-
ishna, and Ariel Fuxman. 2024b. Visual program
distillation: Distilling tools and programmatic rea-
soning into vision-language models. In *Proceedings*
of the IEEE/CVF Conference on Computer Vision
and Pattern Recognition, pages 9590–9601. 701
702
703
704
705
706
707

Zhiqiang Hu, Lei Wang, Yihuai Lan, Wanyu Xu, Ee-
Peng Lim, Lidong Bing, Xing Xu, Soujanya Po-
ria, and Roy Ka-Wei Lee. 2023. Llm-adapters:
An adapter family for parameter-efficient fine-
tuning of large language models. *arXiv preprint*
arXiv:2304.01933. 708
709
710
711
712
713

Mingxin Huang, Yongxin Shi, Dezhi Peng, Songxuan
Lai, Zecheng Xie, and Lianwen Jin. 2025a. Ocr-
reasoning benchmark: Unveiling the true capabili-
ties of mllms in complex text-rich image reasoning.
arXiv preprint arXiv:2505.17163. 714
715
716
717
718

719	Zeyi Huang, Yuyang Ji, Anirudh Sundara Rajan, Zefan Cai, Wen Xiao, Haohan Wang, Junjie Hu, and Yong Jae Lee. 2025b. Visualtoolagent (vista): A reinforcement learning framework for visual tool selection. <i>arXiv preprint arXiv:2505.20289</i> .	774
720		775
721		776
722		777
723		778
724	Hugging Face. 2025. Open r1: A fully open reproduction of deepseek-r1 .	779
725		780
726	Aaron Hurst, Adam Lerer, Adam P Goucher, Adam Perelman, Aditya Ramesh, Aidan Clark, AJ Ostrow, Akila Welihinda, Alan Hayes, Alec Radford, and 1 others. 2024. Gpt-4o system card. <i>arXiv preprint arXiv:2410.21276</i> .	781
727		782
728		
729		
730		
731	Bo Li, Yuanhan Zhang, Dong Guo, Renrui Zhang, Feng Li, Hao Zhang, Kaichen Zhang, Peiyuan Zhang, Yanwei Li, Ziwei Liu, and 1 others. 2024. Llava-onevision: Easy visual task transfer. <i>arXiv preprint arXiv:2408.03326</i> .	783
732		784
733		785
734		786
735		
736	Junnan Li, Dongxu Li, Silvio Savarese, and Steven Hoi. 2023. Blip-2: Bootstrapping language-image pre-training with frozen image encoders and large language models. In <i>International conference on machine learning</i> , pages 19730–19742. PMLR.	787
737		788
738		789
739		790
740		
741	Wentong Li, Yuqian Yuan, Jian Liu, Dongqi Tang, Song Wang, Jie Qin, Jianke Zhu, and Lei Zhang. 2025a. Tokenpacker: Efficient visual projector for multimodal llm. <i>International Journal of Computer Vision</i> , pages 1–19.	791
742		792
743		793
744		794
745		795
746	Xinhao Li, Ziang Yan, Desen Meng, Lu Dong, Xiangyu Zeng, Yinan He, Yali Wang, Yu Qiao, Yi Wang, and Limin Wang. 2025b. Videochat-r1: Enhancing spatio-temporal perception via reinforcement fine-tuning. <i>arXiv preprint arXiv:2504.06958</i> .	796
747		797
748		798
749		799
750		800
751	Xuchen Li, Xuzhao Li, Shiyu Hu, Kaiqi Huang, and Wentao Zhang. 2025c. Causalstep: A benchmark for explicit stepwise causal reasoning in videos. <i>arXiv preprint arXiv:2507.16878</i> .	801
752		802
753		803
754		804
755	Xuzhao Li, Xuchen Li, Shiyu Hu, Yongzhen Guo, and Wentao Zhang. 2025d. Verifybench: A systematic benchmark for evaluating reasoning verifiers across domains. <i>arXiv preprint arXiv:2507.09884</i> .	805
756		806
757		807
758		808
759	Yuting Li, Lai Wei, Kaipeng Zheng, Jingyuan Huang, Linghe Kong, Lichao Sun, and Weiran Huang. 2025e. Vision matters: Simple visual perturbations can boost multimodal math reasoning. <i>arXiv preprint arXiv:2506.09736</i> .	809
760		
761		
762		
763		
764	Haotian Liu, Chunyuan Li, Yuheng Li, Bo Li, Yuanhan Zhang, Sheng Shen, and Yong Jae Lee. 2024. Llava-next: Improved reasoning, ocr, and world knowledge .	810
765		811
766		812
767	Haotian Liu, Chunyuan Li, Qingyang Wu, and Yong Jae Lee. 2023. Visual instruction tuning.	813
768		814
769	Xiangyan Liu, Jinjie Ni, Zijian Wu, Chao Du, Longxu Dou, Haonan Wang, Tianyu Pang, and Michael Qizhe Shieh. 2025. Noisyrollout: Reinforcing visual reasoning with data augmentation. <i>arXiv preprint arXiv:2504.13055</i> .	815
770		816
771		817
772		818
773		819
		820
		821
		822
		823
		824
		825
		826
	Haoyu Lu, Wen Liu, Bo Zhang, Bingxuan Wang, Kai Dong, Bo Liu, Jingxiang Sun, Tongzheng Ren, Zhuoshu Li, Hao Yang, and 1 others. 2024. Deepseek-vl: towards real-world vision-language understanding. <i>arXiv preprint arXiv:2403.05525</i> .	
	Pan Lu, Bowen Chen, Sheng Liu, Rahul Thapa, Joseph Boen, and James Zou. 2025. Octotools: An agentic framework with extensible tools for complex reasoning. <i>arXiv preprint arXiv:2502.11271</i> .	
	Haohao Luo, Yang Deng, Ying Shen, See-Kiong Ng, and Tat-Seng Chua. 2024. Chain-of-exemplar: Enhancing distractor generation for multimodal educational question generation. <i>ACL</i> .	
	Yingzi Ma, Yulong Cao, Jiachen Sun, Marco Pavone, and Chaowei Xiao. 2024. Dolphins: Multimodal language model for driving. In <i>European Conference on Computer Vision</i> , pages 403–420. Springer.	
	Minesh Mathew, Viraj Bagal, Rubèn Tito, Dimosthenis Karatzas, Ernest Valveny, and CV Jawahar. 2022. Infographicvqa. In <i>Proceedings of the IEEE/CVF Winter Conference on Applications of Computer Vision</i> , pages 1697–1706.	
	Haozhan Shen, Kangjia Zhao, Tiancheng Zhao, Ruo Chen Xu, Zilun Zhang, Mingwei Zhu, and Jianwei Yin. 2024. Zoomeye: Enhancing multimodal llms with human-like zooming capabilities through tree-based image exploration. <i>arXiv preprint arXiv:2411.16044</i> .	
	Yiqing Shen, Chenjia Li, Chenxiao Fan, and Mathias Unberath. 2025. Rvtbench: A benchmark for visual reasoning tasks. <i>arXiv preprint arXiv:2505.11838</i> .	
	Kunpeng Song, Yizhe Zhu, Bingchen Liu, Qing Yan, Ahmed Elgammal, and Xiao Yang. 2024. Moma: Multimodal llm adapter for fast personalized image generation. In <i>European Conference on Computer Vision</i> , pages 117–132. Springer.	
	Alex Su, Haozhe Wang, Weiming Ren, Fangzhen Lin, and Wenhui Chen. 2025. Pixel reasoner: Incentivizing pixel-space reasoning with curiosity-driven reinforcement learning. <i>arXiv preprint arXiv:2505.15966</i> .	
	Cheng Tan, Jingxuan Wei, Zhangyang Gao, Linzhuang Sun, Siyuan Li, Ruifeng Guo, Bihui Yu, and Stan Z Li. 2023. Boosting the power of small multimodal reasoning models to match larger models with self-consistency training. <i>arXiv preprint arXiv:2311.14109</i> .	
	Gemini Team, Rohan Anil, Sebastian Borgeaud, Jean-Baptiste Alayrac, Jiahui Yu, Radu Soricut, Johan Schalkwyk, Andrew M Dai, Anja Hauth, Katie Millican, and 1 others. 2023. Gemini: a family of highly capable multimodal models. <i>arXiv preprint arXiv:2312.11805</i> .	

827	Gemini Team, Petko Georgiev, Ving Ian Lei, Ryan Burnell, Libin Bai, Anmol Gulati, Garrett Tanzer, Damien Vincent, Zhufeng Pan, Shibo Wang, and 1 others. 2024. Gemini 1.5: Unlocking multimodal understanding across millions of tokens of context. <i>arXiv preprint arXiv:2403.05530</i> .	Large multimodal model as open and versatile visual relationship generalist. <i>IEEE Transactions on Pattern Analysis and Machine Intelligence</i> .	882 883 884
833	Gemma Team, Aishwarya Kamath, Johan Ferret, Shreya Pathak, Nino Vieillard, Ramona Merhej, Sarah Perrin, Tatiana Matejovicova, Alexandre Ramé, Morgane Rivière, and 1 others. 2025. Gemma 3 technical report. <i>arXiv preprint arXiv:2503.19786</i> .	Qinghao Ye, Haiyang Xu, Guohai Xu, Jiabo Ye, Ming Yan, Yiyang Zhou, Junyang Wang, Anwen Hu, Pengcheng Shi, Yaya Shi, and 1 others. 2023. mplug-owl: Modularization empowers large language models with multimodality. <i>arXiv preprint arXiv:2304.14178</i> .	885 886 887 888 889 890
838	Peng Wang, Shuai Bai, Sinan Tan, Shijie Wang, Zhihao Fan, Jinze Bai, Keqin Chen, Xuejing Liu, Jialin Wang, Wenbin Ge, and 1 others. 2024a. Qwen2-vl: Enhancing vision-language model's perception of the world at any resolution. <i>arXiv preprint arXiv:2409.12191</i> .	Qinghao Ye, Haiyang Xu, Jiabo Ye, Ming Yan, Anwen Hu, Haowei Liu, Qi Qian, Ji Zhang, and Fei Huang. 2024. mplug-owl2: Revolutionizing multi-modal large language model with modality collaboration. In <i>Proceedings of the IEEE/CVF conference on computer vision and pattern recognition</i> , pages 13040–13051.	891 892 893 894 895 896
844	Song Wang, Gongfan Fang, Lingdong Kong, Xiangtai Li, Jianyun Xu, Sheng Yang, Qiang Li, Jianke Zhu, and Xinchao Wang. 2025a. Pixelthink: Towards efficient chain-of-pixel reasoning. <i>arXiv preprint arXiv:2505.23727</i> .	Daoan Zhang, Junming Yang, Hanjia Lyu, Zijian Jin, Yuan Yao, Mingkai Chen, and Jiebo Luo. 2024. Cocot: Contrastive chain-of-thought prompting for large multimodal models with multiple image inputs. <i>arXiv preprint arXiv:2401.02582</i> .	897 898 899 900 901
849	Weiyun Wang, Zhangwei Gao, Lixin Gu, Hengjun Pu, Long Cui, Xingguang Wei, Zhaoyang Liu, Linglin Jing, Shenglong Ye, Jie Shao, and 1 others. 2025b. Internvl3. 5: Advancing open-source multimodal models in versatility, reasoning, and efficiency. <i>arXiv preprint arXiv:2508.18265</i> .	Xintong Zhang, Zhi Gao, Bofei Zhang, Pengxiang Li, Xiaowen Zhang, Yang Liu, Tao Yuan, Yuwei Wu, Yunde Jia, Song-Chun Zhu, and 1 others. 2025a. Chain-of-focus: Adaptive visual search and zooming for multimodal reasoning via rl. <i>arXiv preprint arXiv:2505.15436</i> .	902 903 904 905 906 907
855	Wenbin Wang, Liang Ding, Minyan Zeng, Xiabin Zhou, Li Shen, Yong Luo, and Dacheng Tao. 2024b. Divide, conquer and combine: A training-free framework for high-resolution image perception in multimodal large language models. <i>arXiv preprint</i> .	Yi-Fan Zhang, Xingyu Lu, Shukang Yin, Chaoyou Fu, Wei Chen, Xiao Hu, Bin Wen, Kaiyu Jiang, Changyi Liu, Tianke Zhang, and 1 others. 2025b. Thyme: Think beyond images. <i>arXiv preprint arXiv:2508.11630</i> .	908 909 910 911 912
860	Xidong Wang, Dingjie Song, Shunian Chen, Chen Zhang, and Benyou Wang. 2024c. Longllava: Scaling multi-modal llms to 1000 images efficiently via a hybrid architecture. <i>arXiv preprint arXiv:2409.02889</i> .	Zhuosheng Zhang, Aston Zhang, Mu Li, Hai Zhao, George Karypis, and Alex Smola. 2023. Multimodal chain-of-thought reasoning in language models. <i>arXiv preprint arXiv:2302.00923</i> .	913 914 915 916
865	Ye Wang, Qianglong Chen, Zejun Li, Siyuan Wang, Shijie Guo, Zhirui Zhang, and Zhongyu Wei. 2025c. Simple o3: Towards interleaved vision-language reasoning. <i>arXiv preprint arXiv:2508.12109</i> .	Ge Zheng, Bin Yang, Jiajin Tang, Hong-Yu Zhou, and Sibe Yang. 2023. Ddcot: Duty-distinct chain-of-thought prompting for multimodal reasoning in language models. <i>Advances in Neural Information Processing Systems</i> , 36:5168–5191.	917 918 919 920 921
869	Jason Wei, Xuezhi Wang, Dale Schuurmans, Maarten Bosma, Fei Xia, Ed Chi, Quoc V Le, Denny Zhou, and 1 others. 2022. Chain-of-thought prompting elicits reasoning in large language models. <i>Advances in neural information processing systems</i> , 35:24824–24837.	Jinliang Zheng, Jianxiong Li, Sijie Cheng, Yinan Zheng, Jiaming Li, Jihao Liu, Yu Liu, Jingjing Liu, and Xianyu Zhan. 2024. Instruction-guided visual masking. <i>Advances in neural information processing systems</i> , 37:126004–126031.	922 923 924 925 926
875	Penghao Wu and Saining Xie. 2024. V?: Guided visual search as a core mechanism in multimodal llms. In <i>Proceedings of the IEEE/CVF Conference on Computer Vision and Pattern Recognition</i> , pages 13084–13094.	Ziwei Zheng, Michael Yang, Jack Hong, Chenxiao Zhao, Guohai Xu, Le Yang, Chao Shen, and Xing Yu. 2025. Deepeyes: Incentivizing "thinking with images" via reinforcement learning. <i>arXiv preprint arXiv:2505.14362</i> .	927 928 929 930 931
880	Chi Xie, Shuang Liang, Jie Li, Zhao Zhang, Feng Zhu, Rui Zhao, and Yichen Wei. 2025. Relationlmm:	Zetong Zhou, Dongping Chen, Zixian Ma, Zhihan Hu, Mingyang Fu, Sinan Wang, Yao Wan, Zhou Zhao, and Ranjay Krishna. 2025. Reinforced visual perception with tools. <i>Preprint</i> , arXiv:2509.01656.	932 933 934 935

936 Jinguo Zhu, Weiyun Wang, Zhe Chen, Zhaoyang Liu,
937 Shenglong Ye, Lixin Gu, Hao Tian, Yuchen Duan,
938 Weijie Su, Jie Shao, and 1 others. 2025. Internvl3:
939 Exploring advanced training and test-time recipes
940 for open-source multimodal models. *arXiv preprint*
941 *arXiv:2504.10479*.

Appendix

A Detailed Prompts

We provide the exact prompts used in different training phases. Specifically, the SFT stage uses the instruction template in Prompt 1, which aims to establish foundational competence in both pure textual CoT and the proper execution of visual operations. In the RL stage, the prompts for pixel necessity estimation rollouts enforce opposite behaviors: Prompt 2 explicitly instructs the model to invoke zoom-in, while Prompt 3 prohibits its use. These controlled settings enable the model to learn the correspondence between query type and tool necessity. In contrast, the adaptive rollout phase adopts the neutral prompt in Prompt 4, where the model is free to decide whether or not to perform pixel-space reasoning. This setup ensures that the model is first exposed to both extremes during necessity estimation and then given autonomy to balance textual reasoning and visual operations during adaptive rollouts.

B Training Hyperparameters

Table A1 and A2 summarize the key hyperparameters for both the supervised fine-tuning (SFT) and reinforcement learning (RL) stages. The SFT phase initializes the model with baseline competence in pure textual CoT and pixel-space operations, specifying optimizer, learning rate schedule, batch sizes and frozen vision modules.

The RL phase trains the model for adaptive tool usage through rollout-guided reinforcement learning. Key settings include global and micro batch sizes, replay buffer size, number of samples and episodes, input/output lengths, learning rate, KL coefficient, train temperature, top-p sampling, reward and its coefficients.

C Benchmark Details

We evaluate our method across five diverse multimodal benchmarks, covering both fine-grained perception and complex high-level reasoning. V* (V-Star) Bench (Wu and Xie, 2024) assesses the ability of VLMs to handle visually intricate, high-resolution images and capture subtle details. MMStar (Chen et al., 2024) focuses on general-purpose multimodal reasoning, testing comprehension across a broad set of tasks involving textual and visual interactions. HR-Bench (Wang et al.,

2024b) (HR-Bench 4K/8K) are specifically designed to probe the capability of models in dealing with ultra-high-resolution images, where reasoning often requires identifying small-scale objects or subtle visual cues that are easily overlooked. Finally, InfographicVQA (InfoVQA) (Mathew et al., 2022) emphasizes reasoning over infographic-style images that tightly integrate diagrams, charts, and textual annotations, requiring precise alignment between textual information and visual layout.

D More Cases

To complement the main experiments, we provide additional qualitative comparisons in Figure A1–A6. These cases illustrate how our model adapts its tool usage across different scenarios. They serve as concrete examples to better understand the model’s reasoning behaviors beyond aggregate metrics.

Figure A1 illustrates two representative cases. On the left, for archaeological site sign text recognition, Pixel Reasoner conducts redundant cropping operations, introducing interfering visual information and thus failing to identify the correct text. In contrast, our model focuses on the key sign, clearly recognizing the text and outputting the correct answer “ISTRE.PULA” without unnecessary steps. On the right, for cricket statistics comparison, Pixel Reasoner makes multiple incorrect crops and miscalculates, while our model accurately locates the relevant statistics in the infographic and solves the task directly, yielding the correct answer “95”. These cases show that our adaptive framework improves efficiency by avoiding unnecessary operations and enhances robustness by making more reliable tool-use decisions.

Figure A2 displays a case from the license plate recognition task, illustrating the reasoning processes of Pixel Reasoner and our method. The goal is to determine the license plate number of the vehicle in the image among the provided options. Pixel Reasoner makes multiple attempts at cropping, first focusing on irrelevant pavement areas before eventually finding the van and its license plate. Our method, however, efficiently zooms in on the van in a single cropping step, directly retrieving the correct license plate number “V-223-LV”. This case exemplifies how our approach optimizes tool utilization for more efficient and precise multimodal reasoning in the context of this case study.

Figure A3 presents a case from the task of de-

Prompt 1: SFT Prompt

You are a helpful assistant.

Tools

You may call one or more functions to assist with the user query.

You are provided with function signatures within `<tools></tools>` XML tags: `<tools>{"type": "function", "function": {"name": "crop_image_normalized", "description": "Zoom in on the image based on the bounding box coordinates. It is useful when the object or text in the image is too small to be seen.", "parameters": {"type": "object", "properties": {"bbox_2d": {"type": "array", "description": "coordinates for bounding box of the area you want to zoom in. Values should be within [0.0,1.0].", "items": {"type": "number"}}, "target_image": {"type": "number", "description": "The index of the image to crop. Index from 1 to the number of images. Choose 1 to operate on original image."}, "required": ["bbox_2d", "target_image"]}}}</tools>`

For each function call, return a json object with function name and arguments within `<tool_call></tool_call>` XML tags: `<tool_call>{"name": <function-name>, "arguments": <args-json-object>} </tool_call>`

[image]

[question]

Guidelines: Understand the given visual information and the user query. Determine if it is beneficial to employ the given visual operations (tools). We can look closer by `crop_image`. Reason with the visual information step by step, and put your final answer within `\boxed{}`.

Prompt 2: RL Prompt for Tool Use in Pixel Necessity Rollouts

You are a helpful assistant.

Tools

You may call one or more functions to assist with the user query.

You are provided with function signatures within `<tools></tools>` XML tags: `<tools>{"type": "function", "function": {"name": "crop_image_normalized", "description": "Zoom in on the image based on the bounding box coordinates. It is useful when the object or text in the image is too small to be seen.", "parameters": {"type": "object", "properties": {"bbox_2d": {"type": "array", "description": "coordinates for bounding box of the area you want to zoom in. Values should be within [0.0,1.0].", "items": {"type": "number"}}, "target_image": {"type": "number", "description": "The index of the image to crop. Index from 1 to the number of images. Choose 1 to operate on original image."}, "required": ["bbox_2d", "target_image"]}}}</tools>`

For each function call, return a json object with function name and arguments within `<tool_call></tool_call>` XML tags: `<tool_call>{"name": <function-name>, "arguments": <args-json-object>} </tool_call>`

[image]

[question]

Guidelines: Understand the given visual information and the user query. You must zoom in on the image using the tool (`crop_image`). Reason with the visual information step by step, and put your final answer within `\boxed{}`.

Prompt 3: RL Prompt for No Tool Use in Pixel Necessity Rollouts

You are a helpful assistant.

[image]

[question]

Guidelines: Understand the given visual information and the user query. Reason with the visual information step by step, and put your final answer within `\boxed{}`.

Prompt 4: RL Prompt for Adaptive Tool Use in Adaptive Rollouts

You are a helpful assistant.

Tools

You may call one or more functions to assist with the user query.

You are provided with function signatures within `<tools></tools>` XML tags: `<tools>{“type”: “function”, “function”:
{“name”: “crop_image_normalized”, “description”: “Zoom in on the image based on the bounding box coordinates. It
is useful when the object or text in the image is too small to be seen.”, “parameters”: {“type”: “object”, “properties”:
{“bbox_2d”: {“type”: “array”, “description”: “coordinates for bounding box of the area you want to zoom in. Values
should be within [0.0,1.0]”, “items”: {“type”: “number”}}}, “target_image”: “type”: “number”, “description”: “The
index of the image to crop. Index from 1 to the number of images. Choose 1 to operate on original image.”}, “required”:
[“bbox_2d”, “target_image”]}}}</tools>`

For each function call, return a json object with function name and arguments within `<tool_call></tool_call>`
XML tags: `<tool_call>{“name”: <function-name>, “arguments”: <args-json-object>} </tool_call>`

[image]

[question]

Guidelines: Understand the given visual information and the user query. Determine if it is beneficial to employ
the given visual operations (tools). We can look closer by crop_image. Reason with the visual information step by step, and
put your final answer within `\boxed{}`.

Table A1: SFT and RL hyperparameters.

Parameter	Value	Parameter	Value
Number of nodes	1	Training batch size (global)	256
GPUs per node	8	Micro batch size (per actor)	2
Total epochs	5	Replay buffer size	512
Seed	49	Rollout batch size	512
Optimizer	AdamW	Number of samples per prompt	16
Learning rate	1.0×10^{-6}	Number of epochs	3
Scheduler	Cosine decay	Max input length	2048
Warmup ratio	0.1	Max generation length	10000
Per-device batch size	1	Actor learning rate	1.0×10^{-6}
Gradient accumulation steps	2	Zero Redundancy Stage	3
Precision	bfloat16 (BF16)	Auxiliary loss coefficient	0.05
Gradient checkpointing	Enabled	KL coefficient	0.0
Attention implementation	FlashAttention-2	Train Temperature	1.0
Freeze vision modules	True	Top-p	0.95
		Precision	bfloat16 (BF16)
		Gradient checkpointing	Enabled
		Attention implementation	FlashAttention

(a) SFT hyperparameters

(b) RL hyperparameters

termining the year Sachin Tendulkar reached the Guinness World Record for being the first player to score 10,000 runs, comparing the reasoning processes of Pixel Reasoner and our method. Pixel Reasoner attempts to zoom in on a section of the infographic’s timeline but ends up with an incorrect year, 2005. Our method, on the other hand, directly analyzes the infographic’s content and ac-

curately identifies the correct year, 2001, without unnecessary tool-based cropping. This case demonstrates the effectiveness of our approach in efficiently and accurately reasoning about such sports-related milestone-finding tasks compared to Pixel Reasoner.

As shown in Figure A4, it presents a case from the task of identifying which two numbered loca-

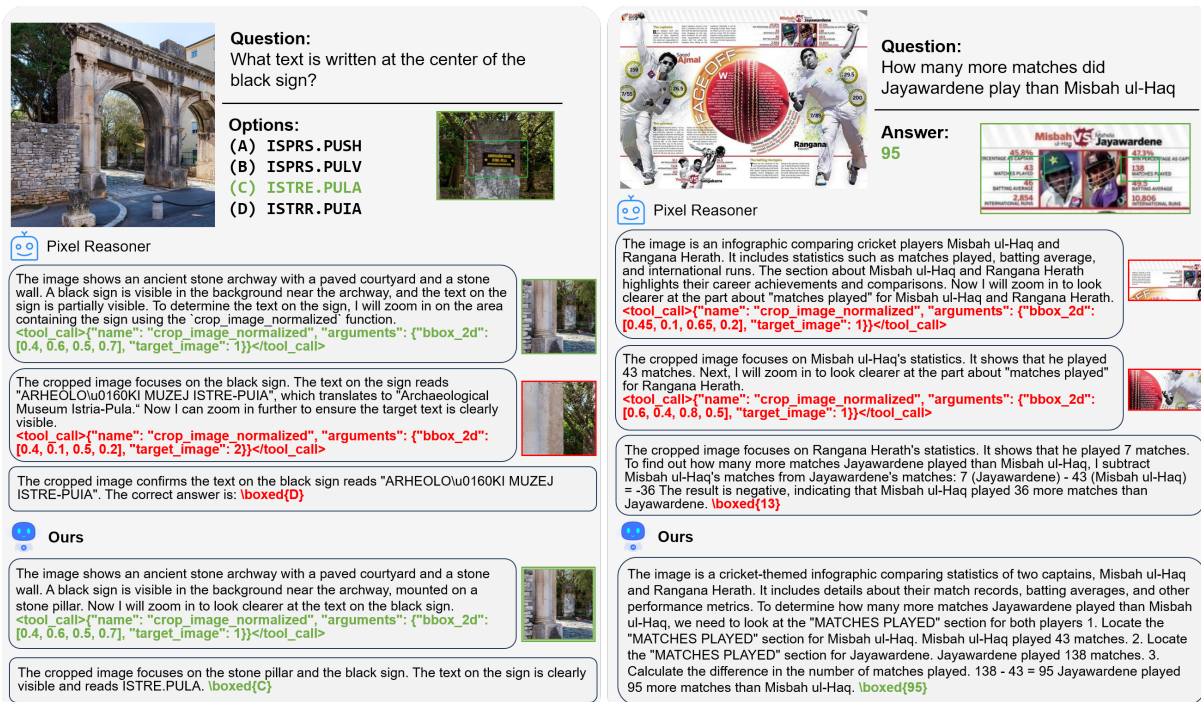


Figure A1: Comparison between Pixel Reasoner and our method on multimodal reasoning tasks. Left: Archaeological site sign text recognition. Right: Cricket statistics comparison.

Table A2: RL reward and its coefficients.

Category	Setting
Pixel Necessity	$b_1: 1.2$
	$c_1: 1.0$
	$\lambda_{instr}: 0.08$
Adaptive	$b_2: 1.6$
	$c_2: 0.8$
	$b_3: 1.2$
	$c_3: 1.0$
Rollout Consistency	$\lambda_{align}: 0.05$
	$\gamma: 0.1$

1055 tions on a provided map belong to the same country,
 1056 comparing the reasoning processes of Pixel Reasoner
 1057 and our method. Pixel Reasoner zooms in on
 1058 the map and incorrectly concludes that locations 2
 1059 and 3 belong to the same country, selecting option
 1060 B. Our method, through analyzing the geographical
 1061 locations of each numbered marker, accurately
 1062 determines that locations 1 and 2 are both in the
 1063 United Kingdom, thus selecting the correct option
 1064 C. This case illustrates how our approach excels
 1065 in precise geographical reasoning and correct option
 1066 selection compared to Pixel Reasoner in such

map-based country association tasks, highlighting
 the latter's error in misidentifying the affiliation of
 location 3.

As shown in Figure A5, it presents a case from
 the task of determining how many types of bonding
 exist in chemistry, comparing the reasoning
 processes of Pixel Reasoner and our method. Pixel
 Reasoner zooms in on a section of the "Map of
 Chemistry" but only identifies two types of bonding
 (covalent and ionic), leading to an incorrect
 answer of 2. Our method, by strategically locating
 the "BONDS" section in the lower-left part of the
 infographic, accurately identifies four types of
 bonding: Covalent Bond, Ionic Bond, van der Waals
 bonding, and Hydrogen Bond, thus obtaining the
 correct answer of 4. This case demonstrates how
 our approach enables more comprehensive and
 accurate information retrieval in chemical concept-
 related reasoning tasks compared to Pixel Reasoner.

For coronavirus-related geographic reasoning in
 Figure A6, Pixel Reasoner engages in two crop
 attempts yet fails to zero in on the correct location
 each time. This points to a tendency of invoking
 the cropping tool in a mechanical, almost obligatory
 manner—"calling the tool just for the sake of tool
 invocation"—without a strategic, solution-oriented
 assessment of when and where to crop. In contrast,
 our model accurately targets the key geographic



Question:

What is the license plate number of the vehicle in the image?

Options:

- (A) V-223-LV
- (B) V-322-LV
- (C) V-224-LV
- (D) V-223-LW



Pixel Reasoner

The image shows a docked ship with a paved area beside it. A van is parked near the ship, and its license plate is visible. The license plate appears to be partially obscured, but the visible portion matches the format of a Dutch license plate. Now I will zoom in to look clearer at the license plate.

`<tool_call>{"name": "crop_image_normalized", "arguments": {"bbox_2d": [0.75, 0.8, 0.85, 0.9], "target_image": 1}}</tool_call>`



The cropped image focuses on the pavement area near the van. The license plate is not visible in this cropped section, indicating that the target image might need further zooming or adjusting. Now I will zoom in again to get a clearer view of the license plate.

`<tool_call>{"name": "crop_image_normalized", "arguments": {"bbox_2d": [0.8, 0.7, 0.9, 0.8], "target_image": 1}}</tool_call>`



The cropped image clearly shows the van and its license plate. The license plate reads **V-223-LV**. `\\boxed{A}`



Ours

The image shows a docked boat with a flag and a paved area. In the background, there is a van parked near a building. The license plate of the van is visible, and the task is to identify its number. Now I will zoom in to look clearer at the license plate of the van.

`<tool_call>{"name": "crop_image_normalized", "arguments": {"bbox_2d": [0.8, 0.7, 0.9, 0.8], "target_image": 1}}</tool_call>`



The cropped image focuses on the van. The license plate clearly displays the number **V-223-LV**. `\\boxed{A}`

Figure A2: Case of license plate recognition task comparison between Pixel Reasoner and our method.

1095 information in a more direct way and produces
1096 the correct answer “Thailand” without redundant
1097 operations.

1098 Through the five case studies (license plate
1099 recognition, Sachin Tendulkar’s record year de-
1100 termination, same-country location identification
1101 on a map, chemical bonding type counting and

coronavirus-related geographic reasoning), we ob-
serve the strengths of our method in adaptive pixel-
space reasoning.

In each case, baselines like Pixel Reasoner ei-
ther overused pixel-level operations (e.g., redun-
dant cropping in license plate recognition and map
tasks, leading to inefficiency or errors) or failed to

1102
1103
1104
1105
1106
1107
1108



Question:

Which year did he reach the Guinness world record for becoming first player to reach 10K runs

Answer:

2001



Pixel Reasoner

The image is an infographic about Sachin Tendulkar, detailing his career highlights, achievements, and personal milestones. It includes timelines, statistics, and quotes about his cricket career. Now I will zoom in to look clearer at the part about "the year he reached the Guinness World Record for becoming the first player to reach 10K runs.

`<tool_call>{"name": "crop_image_normalized", "arguments": {"bbox_2d": [0.16, 0.6, 0.22, 0.7], "target_image": 1}}</tool_call>`



The cropped image focuses on the timeline of Tendulkar's career. The section mentions that he became the first player to score 10,000 runs in ODIs on October 5, 2012. **boxed{2005}**

Ours

The image is an infographic about Sachin Tendulkar, detailing his career highlights, achievements, and personal milestones. It includes timelines, statistics, and quotes about his cricket career. To determine the year he reached the Guinness World Record for being the first player to reach 10,000 runs, I'll look for a specific section in the infographic that mentions this milestone. **boxed{2001}**

Figure A3: Case of Sachin Tendulkar’s Guinness World Record year determination task comparison between Pixel Reasoner and our method.

1109 invoke visual inspection when necessary (missing
1110 critical visual cues, as seen in the chemical bonding
1111 task where Pixel Reasoner identified only partial
1112 bonding types).

1113 In contrast, our model adaptively decides when
1114 to perform fine-grained visual operations (e.g., tar-
1115 geted zoom-in for license plate recognition, direct
1116 content analysis for cricket statistics and chemi-
1117 cal bonding) or rely on semantic reasoning. By
1118 combining operation-aware supervised fine-tuning
1119 and rollout-guided reinforcement learning, it bal-
1120 ances the need for pixel-level operations and high-
1121 level reasoning: it avoids overusing compute-
1122 intensive pixel operations while capturing criti-
1123 cal visual details. This adaptive strategy, guided
1124 by rewards for correctness, instruction-following,
1125 adaptive tool-necessity alignment, and rollout con-
1126 sistency, achieves accurate results across diverse

1127 multimodal reasoning tasks—from visual identifi-
1128 cation to knowledge-based querying—surpassing
1129 both general VLMs and tool-augmented baselines,
1130 and validating the effectiveness of adaptive pixel-
1131 space reasoning.



Question:

On the provided map, which two numbered locations belong to the same country?

Options:

- (A) Locations 2 and 4
- (B) Locations 2 and 3
- (C) Locations 1 and 2
- (D) Locations 1 and 3



Pixel Reasoner

The image is a world map highlighting specific regions with numbered markers. The numbered locations are positioned in Europe, with some overlapping or close proximity. Now I will zoom in to look clearer at the locations numbered 1, 2, 3, and 4.

```
<tool_call>{"name": "crop_image_normalized", "arguments": {"bbox_2d": [0.4, 0.2, 0.5, 0.3], "target_image": 1}}</tool_call>
```



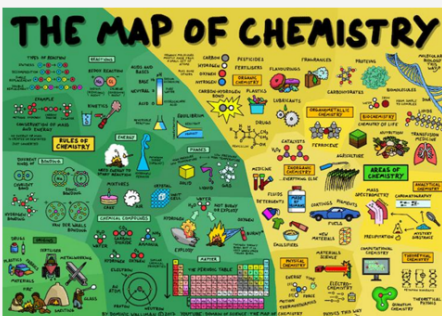
The cropped image focuses on the northern part of Europe, specifically the British Isles. Locations 2 and 3 are marked on the British Isles, which are part of the same country, the United Kingdom. **boxed{B}**



Ours

The image is a world map highlighting specific regions with numbered markers. The numbers (1, 2, 3, 4) are placed over geographical locations, likely representing significant points or countries. To determine which two locations belong to the same country, I need to identify the countries associated with each numbered location: Location 1 is in the northern part of Europe, specifically in the United Kingdom. Location 2 is also in the northern part of Europe, specifically in the United Kingdom. Location 3 is in the northern part of Europe, specifically in Norway. Location 4 is in the northern part of Europe, specifically in Denmark. Both locations 1 and 2 are in the United Kingdom, which explains their proximity and shared characteristics. **boxed{C}**

Figure A4: Case of identifying same-country locations on a map: Comparison between Pixel Reasoner and our method.

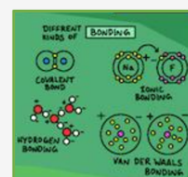


Question:

How many types of bonding are there in chemistry?

Answer:

4



Pixel Reasoner

The image is a colorful and detailed "Map of Chemistry" that illustrates various concepts, rules, and areas of chemistry. It includes sections on types of reactions, rules of chemistry, bonding, and different areas of chemistry. Now I will zoom in to look clearer at the part about "types of bonding."

`<tool_call>{"name": "crop_image_normalized", "arguments": {"bbox_2d": [0.01, 0.4, 0.2, 0.5], "target_image": 1}}</tool_call>`



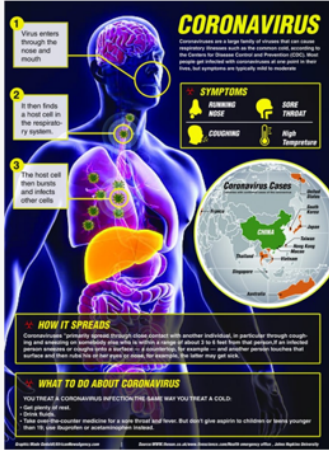
The cropped image focuses on "Rules of Chemistry," specifically highlighting "Different kinds of Bonding." It lists two types of bonding: covalent and ionic. **boxed{2}**



Ours

The image is a colorful and detailed "Map of Chemistry" that illustrates various concepts, rules, and areas of chemistry. It includes sections on chemical reactions, types of bonds, the periodic table, and different areas of chemistry. To determine the number of types of bonding in chemistry, I'll look for the section labeled "BONDS" in the image. 1. Locate the "BONDS" section in the image. 2. Identify the types of bonds listed there. The "BONDS" section is located in the lower-left part of the image. It lists the following types of bonds: Covalent Bond, Ionic Bond, van der Waals bonding, Hydrogen Bond. There are four types of bonds listed in this section. **boxed{4}**

Figure A5: Case of determining the number of chemical bonding types: Comparison between Pixel Reasoner and our method.



Question:
Which country is shown in this infographic, right below china, on the left side?

Answer:
thailand



Pixel Reasoner

The document is an infographic about the coronavirus, detailing its spread, symptoms, and treatment. It includes a section on how the virus spreads, listing countries with confirmed cases. Now I will zoom in to look clearer at the part about "the country shown in this infographic, right below China, on the left side."

`<tool_call>{"name": "crop_image_normalized", "arguments": {"bbox_2d": [0.4, 0.6, 0.6, 0.7], "target_image": 1}}</tool_call>`



The cropped image focuses on the section about "How it Spreads," but the target country is not visible here. I will zoom in further to locate the target country.

`<tool_call>{"name": "crop_image_normalized", "arguments": {"bbox_2d": [0.4, 0.7, 0.99, 0.8], "target_image": 1}}</tool_call>`



The cropped image clearly shows the map of countries with confirmed coronavirus cases. Directly below China, on the left side, is the country Thailand. **boxed{Thailand}**



Ours

The document is an infographic about the coronavirus, detailing its spread, symptoms, and treatment. It includes a section on how the virus spreads, listing countries affected by the virus. The question asks for the country immediately below China on the left side of the infographic. Key Observations: 1. The infographic includes a map of the world with highlighted countries affected by the coronavirus. 2. The map is positioned to the right of the central illustration of the human body. 3. The countries are listed in a clockwise direction from China. Step-by-Step Reasoning: 1. Locate China on the map. 2. Identify the country directly below China. 3. The map shows Thailand positioned directly below China. **boxed{Thailand}**

Figure A6: Case of coronavirus-related geographic reasoning: Comparison between Pixel Reasoner and our method.